Validation of v1.022 mesospheric water vapor observed by the Solar Occultation for Ice Experiment instrument on the Aeronomy of Ice in the Mesosphere satellite

Pingping Rong,[1] James M. Russell III,[1] Larry L. Gordley,[2] Mark E. Hervig,[3] Lance Deaver,[2] Peter F. Bernath,[4] and Kaley A. Walker[5]

Received 26 March 2010; revised 29 August 2010; accepted 3 September 2010; published 30 December 2010.

[1] Water vapor measured by the Solar Occultation for Ice Experiment (SOFIE) instrument on the Aeronomy of Ice in the Mesosphere satellite has been validated in the vertical range 45–95 km. Precision estimates for SOFIE v1.022 H_2O are ~0.2%–2.5% up to 80 km and degrade to ~20% at ~90 km. The SOFIE total systematic error from the retrieval analysis remains at ~3%–4% throughout the lower to middle mesosphere and increases from ~9% at 85 km to ~16% at 95 km. Comparisons with Atmospheric Chemistry Experiment-Fourier Transform Spectrometer (ACE-FTS) and Microwave Limb Sounder (MLS) H_2O show excellent agreement (0%–2%) up to 80 km in the Northern Hemisphere with rare exceptions. Percentage differences above ~85 km increase to ~20% or worse due largely to the low H_2O volume mixing ratios in the upper mesosphere. For the Southern Hemisphere SOFIE is consistently biased low by 10%–20% relative to both ACE-FTS and MLS H_2O. Slopes of SOFIE daily mean H_2O isopleths on an altitude versus time cross section are used as an indicator of upwelling air motion. In the lower to middle mesosphere, the slope is the largest from mid-May to mid-June (maximum of ~1.5 cm/s), and then in July and August, it is reduced significantly. Both SOFIE and MLS daily mean H_2O volume mixing ratios at the polar mesospheric cloud height increase rapidly from ~2.0 to ~5.0 ppmv prior to the solstice and then approach a near-constant but slightly increasing level (6.0–6.5 ppmv) throughout the season.

Citation: Rong, P. P., J. M. Russell III, L. L. Gordley, M. E. Hervig, L. Deaver, P. F. Bernath, and K. A. Walker (2010), Validation of v1.022 mesospheric water vapor observed by the Solar Occultation for Ice Experiment instrument on the Aeronomy of Ice in the Mesosphere satellite, *J. Geophys. Res.*, *115*, D24314, doi:10.1029/2010JD014269.

1. Introduction

[2] Water vapor (H_2O) volume mixing ratios (vmrs) in the polar mesosphere during summer are significantly enhanced relative to other seasons. This enhancement is of critical importance to the existence of polar mesospheric clouds (PMCs) and is primarily caused by upwelling air motion that is associated with the meridional circulation driven by mesospheric gravity wave drag [e.g., *Garcia and Solomon*, 1985]. This summertime enhancement provides an especially favorable condition for PMCs to form when combined with an extremely cold summer mesopause (with T of ~120–150 K). The low temperature results in an extremely low H_2O saturation pressure (i.e., P_{sat} decreases exponentially as $1/T$ increases linearly), and therefore, the atmosphere is more apt to achieve a supersaturated state ($P_{H2O}/P_{sat} \geq 1$, where P_{H2O} is the H_2O partial pressure). In the upper mesosphere and lower thermosphere (i.e., >80 km) H_2O decreases rapidly owing to its significantly shortened photochemical life time (i.e., a few days). In addition, between the mesopause and PMC altitudes, the production of ice particles also takes away some amount of water vapor.

[3] The Solar Occultation for Ice Experiment (SOFIE) is one of the three instruments aboard the Aeronomy of Ice in the Mesosphere (AIM) satellite, all of which are dedicated to the study of polar mesospheric clouds. SOFIE retrieved products include temperature (T), volume mixing ratios (vmrs) of water vapor (H_2O), ozone (O_3), nitric oxide (NO), methane (CH_4), carbon dioxide (CO_2), and PMC particle characteristics such as mass or number density and size distribution [*Gordley et al.*, 2009; *Hervig et al.*, 2009]. The vertical range of SOFIE H_2O in the v1.022 release extends from 95 km down to the lower stratosphere at ~15 km. We focus on the 45–95 km range in this paper.

[4] The current study has a twofold purpose. The first is to perform contemporary comparisons of H_2O profiles between SOFIE and several other satellite data sets, and the

[1]Center for Atmospheric Sciences, Hampton University, Hampton, Virginia, USA.
[2]GATS, Inc., Newport News, Virginia, USA.
[3]GATS, Inc., Driggs, Idaho, USA.
[4]Department of Chemistry, University of York, York, UK.
[5]Department of Physics, University of Toronto, Toronto, Ontario, Canada.

0148-0227/10/2010JD014269

second is to examine the polar summer climatological features shown in SOFIE H_2O. There are only a few satellite instruments to date that have measured or are currently measuring H_2O throughout the mesosphere, including the Halogen Occultation Experiment (HALOE) [*Russell et al.*, 1993] that operated on UARS from 12 September 1991 until 15 December 2005, the Atmospheric Chemistry Experiment-Fourier transform spectrometer (ACE-FTS) [*Bernath et al.*, 2005] on SCISAT-1, the Microwave Limb Sounder (MLS) [*Waters et al.*, 2006] on Aura, the submillimeter radiometer (SMR) [*Murtagh et al.*, 2002] on Odin, and Sounding of the Atmosphere using Broadband Emission Radiometry (SABER) [*Russell et al.*, 1999] on TIMED. All these instruments, except for HALOE, are still in operation. A recent study by *Stevens et al.* [2008] has shown that mesospheric H_2O can be derived from the OSIRIS/Odin [*Llewellyn et al.*, 2004] level 2 OH 308 nm volume emission rate (VER). Only a limited amount of data is currently available but the new approach points to a potential database for future scientific use. In this paper, we will use ACE-FTS v2.2 and MLS v2.2 H_2O as the primary data sets to make contemporary comparisons with SOFIE H_2O since they are from operational retrievals and have been thoroughly validated [*Carleer et al.*, 2008; *Lambert et al.*, 2007]. Aside from the profile comparisons, we also take a special interest in an enhanced H_2O layer regularly present at ~80 km in SOFIE H_2O. This layer is a well-known feature that has been interpreted by *Summers et al.* [2001] as being caused by a high degree of supersaturation in the PMC region resulting in ice particle formation, sedimentation, and subsequent sublimation at altitudes below the PMC layer. The SOFIE enhancement layer is evaluated against HALOE observations. In section 2, SOFIE H_2O channel characteristics, retrieval algorithms, and error analysis are discussed. In section 3, the correlative data sets used are described. The results of comparisons with the correlative data sets are discussed in section 4. A number of H_2O related polar summer spatial and temporal features are discussed in section 5. Section 6 presents a summary and conclusions.

2. SOFIE H_2O Channel Characteristics, Retrieval Algorithms, and Error Analysis

2.1. SOFIE Measurement Approach

[5] The AIM satellite was launched into a circular 600 km Sun-synchronous polar orbit of 97.8° inclination on 25 April 2007 [*Russell et al.*, 2009]. Consecutive sunrises or sunsets are separated by ~96 min in time or ~24° in longitude. The AIM ascending node equatorial crossing time is at midnight. Spacecraft sunset measurements occur at latitudes between about 65°S and 83°S, and sunrise measurements are between about 65°N and 83°N. AIM is in retrograde orbit and consequently, the precession causes the spacecraft to travel from east to west. Therefore, SOFIE sunsets occur in the Southern Hemisphere (SH) near the time of local sunrise and vice versa for the Northern Hemisphere (NH). All future references to "sunrise" or "sunset" refer to the local time of the measurement. Figure 1 shows the latitude coverage and corresponding local time (LT) of SOFIE measurements. The latitude coverage remains in the polar region north/south of 65°N/S and periodically repeats approximately every 6 months. The local time however repeats approximately every 12 months, i.e., Figure 1b shows that in the NH the local sunset periodically varies between 1300 LT and 2300 LT, whereas in the SH the local sunrise varies between 100 LT and 1100 LT. SOFIE measures vertical profiles of limb path atmospheric transmission $\tau = V/V_0$, with V_0 and V representing the solar intensity measured outside and through the atmosphere, respectively. Eight channels with two spectral bands each are used between 0.29 and 5.26 μm wavelength. In each channel one band is selected in a wavelength region of strong absorption (V_s) and one in a spectrally adjacent region of weaker absorption (V_w) for the target gas. SOFIE measurements are accomplished by monitoring solar intensity as the satellite enters or exits the Earth's shadow. The optical field-of-view (FOV) (2.09 arcmin, equivalent to ~1.6 km at 83 km) and the data sampling rate (20 Hz) are combined to give a vertical resolution of ~2 km for all channels of SOFIE retrievals [*Gordley et al.*, 2009].

2.2. SOFIE H_2O Retrieval

[6] All gas and temperature retrievals in the current v1.022 release are based on the strong band radiometer signals (V_s). Water vapor is retrieved from SOFIE band 6 (strong band of channel 3, centered at 2.618 μm) measurements. The water vapor bands are located at the spectral minimum for ice extinction [see *Gordley et al.*, 2009, Figure 1], thereby providing H_2O extinction measurements that are unaffected by PMCs. The vertical range of current H_2O retrievals is from 15 to 95 km. Future retrievals of H_2O will use the channel 3 difference signals (V_w-V_s or ΔV), which are expected to provide H_2O profiles that will extend to above 100 km altitude.

[7] An "onion-peeling" algorithm is used in the retrieval of each limb profile. A spherically symmetric atmosphere is assumed and divided into a finite number of layers. The vmr of the constituent of interest is inferred successively from the top of the atmosphere to the bottom [*Gordley et al.*, 2009]. The simulated transmissions (V/V_0) are compared to the measured signals, and the target gas mixing ratio is adjusted until the measured transmission is reproduced within the noise level (i.e., inverse of the signal-to-noise ratio, ~10^{-6} for channel 3). To obtain one profile, seven "interleaves" [see e.g., *Remsberg et al.*, 2008] at 1.4 km spacing are performed and the resulting seven profiles are combined to produce a final profile that is reported on a uniform 0.2 km vertical grid. Note that the effective vertical resolution of the measurements is 2 km, as explained above.

2.3. SOFIE H_2O Error Analysis

[8] Errors in the retrieved H_2O stem from the instrument noise, calibration uncertainties, and the retrieval algorithms. Potential error sources are detailed by *Gordley et al.* [2009]. The V and ΔV signals are digitized at 1 kHz using a 14-bit analog-to-digital converter, then averaged to 20 Hz and output at 16 bits. Ground processing further averages the signals to 2 Hz using 32 bit words. This process provides a dynamic range of over 10^6. Signal drifts are measured above the atmosphere and removed to a fraction of the noise level at high altitudes. The H_2O precision (random error) in response to this noise is calculated through retrieval analysis to be about ~0.05 ppmv at ~83 km (i.e., approximately the PMC centroid height).

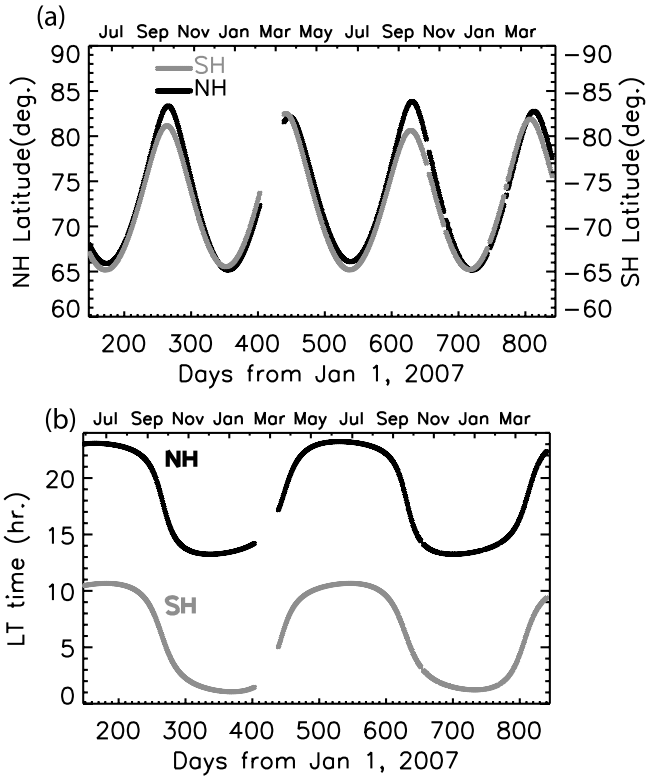

Figure 1. (a) SOFIE latitude coverage and (b) local time (LT) coverage. The black and gray lines are for the Northern Hemisphere and Southern Hemisphere, respectively. The month names are marked in the beginning of each month.

[9] An empirically estimated precision profile was obtained for each SOFIE H_2O profile. The standard deviation of 11 retrieved values (spanning 2 km), i.e., 5 points below, above, and at the given altitude all together, was taken as the precision. The root mean square of a large ensemble of single profile precisions was taken as the estimated precision (Figure 2). This approach ensures that only small scale disturbances on the current vertical profile contribute to the scatter so that the estimated precision is not contaminated by longer or larger scale atmospheric variability. In this paper only profiles in spring and fall (i.e., including March, April, September, and October, over 2000 profiles for each hemisphere) are used because during the equinox period gravity wave activity in the mesosphere is relatively weak compared to the solstice period [e.g., *Garcia and Solomon*, 1985]. Figure 2 indicates extremely high precision, varying gradually from ~0.4% at ~45 km to ~2.5% at ~80 km and then increasing to ~20% (average of the NH and SH) at ~90 km. The precision by vmrs varies from ~0.02 ppmv at ~45 km to ~0.1 ppmv (average of the NH and SH) at ~90 km. The estimated precision at 83 km is ~0.07 ppmv, which is slightly larger but fairly close to the result from the retrieval analysis.

[10] The itemized systematic error responses from the retrieval analysis are listed in Table 1. The analysis started with a simulated radiance profile that was calculated using a typical polar summer H_2O profile. The resulting retrieval from this profile gives us the baseline retrieval. Then we apply small perturbations to several key parameters in the retrieval algorithm that simulate the affects of the different error mechanisms. The differences between the baseline retrieval and the perturbed retrieval provide the error response. In some cases, we determined the 1-σ standard deviation of the differences.

[11] Temperature uncertainty is the leading cause of the systematic error in the SOFIE H_2O retrieval. Since temperature and pressure are retrieved together using CO_2 channels 4 and 7 [*Gordley et al.*, 2009], the error response in H_2O vmr stems from both the temperature itself and the corresponding pressure uncertainty. In the current v1.022, the CO_2 retrieval is not included so the Whole Atmosphere Community Climate Model (WACCM) [*Garcia et al.*, 2007] CO_2 is used to retrieve temperature. SOFIE v1.022 temperature is known to have a warm bias (~5–10 K on average) in the upper mesosphere to lower thermosphere relative to SABER, ACE, and MLS temperature (not shown). The warm bias exists in both hemispheres but the bias in the SH is more significant especially in summer. In reflecting such a vertical distribution, a temperature uncertainty is assumed to be zero at 65 km and then it linearly increases to about 6 K at 80 km and remains constant above 80 km. The error response by percentage varies from ~2% at 75 km to ~12% at 95 km; while by vmrs it varies from ~0.14 to ~0.19 ppmv, showing little altitude dependence.

[12] Another primary contributor to the SOFIE H_2O systematic error is the field-of-view (FOV) off-axis correction, which refers to the removal of the far wings of a finite FOV. The SOFIE forward radiance model [*Gordley et al.*, 1994; *Marshall et al.*, 1994] uses an infinitesimal raypath; therefore, the finite FOV effect must be removed. This is performed by convolving the measurement with the FOV and solar disk and using the difference between this result and the original measurement to create corrected signals without FOV effects. The error response from such a removal

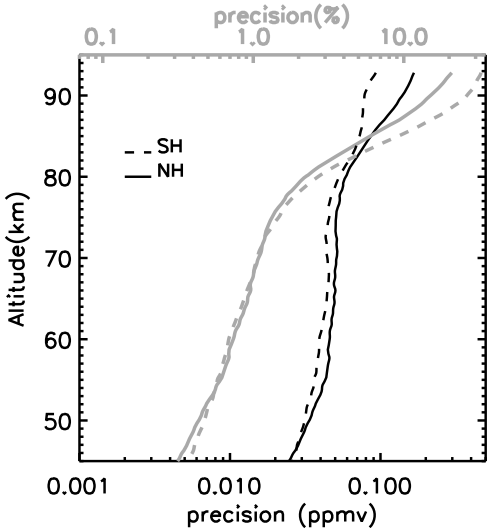

Figure 2. Empirically estimated SOFIE v1.022 H_2O precision, see section 2.3 for detailed description. The NH (2269 profiles) and SH (2319 profiles) are analyzed separately. Precision in units of ppmv and percentage are shown by the black and gray colors, respectively.

Table 1. Random and Systematic Errors for SOFIE v1.022 Water Vapor[a]

Error Mechanism	95 km	85 km	75 km	65 km	55 km	50 km
Random % (ppmv)	27.0 (0.13)	7.6 (0.08)	1.4 (0.05)	0.9 (0.05)	0.6 (0.04)	0.5 (0.03)
Systematic % (ppmv)						
Temperature bias (0–6 K)	12 (0.17)	6 (0.19)	2 (0.14)	0	0	0
Line strengths (1.5%)	1.5 (0.02)	1.5 (0.05)	1.5 (0.11)	1.5 (0.11)	1.5 (0.12)	1.5 (0.12)
Air-broadened half-widths (5%)	<0.1 (<0.01)	<0.1 (<0.01)	<0.1 (<0.01)	<0.1 (<0.01)	1 (<0.01)	1.5 (0.12)
Registration altitude (100 m)	2.5 (0.04)	2 (0.06)	2 (0.14)	1.5 (0.11)	1.5 (0.12)	1.5 (0.12)
Forward model	1 (0.01)	2.5 (0.08)	2 (0.14)	1 (0.07)	0.5 (0.04)	0.5 (0.04)
FOV off-axis correction	10 (0.14)	6 (0.19)	2 (0.14)	2 (0.14)	2 (0.16)	3 (0.24)
Total systematic (root sum square)	16 (0.22)	9 (0.28)	4 (0.28)	3 (0.22)	3 (0.24)	4 (0.32)
Total error (random plus systematic; root sum square)	31.4 (0.26)	11.8 (0.29)	4.2 (0.28)	3.1 (0.23)	3.1 (0.24)	4.0 (0.32)

[a]For each listed altitude, the average of the NH and SH estimated precisions (Figure 2) is taken as the random error. The systematic errors are obtained from the retrieval analysis (see section 2.3 for details).

procedure varies from ~0.14 to 0.24 ppmv, and by percentage it is ~2%–3% below 75 km and reaches ~6%–10% in the upper mesosphere.

[13] SOFIE altitude registration was accomplished by first determining the relative angles between the two consecutive measurements (point-to-point registration) based on the orbital ephemeris and FOV pointing knowledge and then obtaining the absolute altitudes by comparing the modeled and measured CO_2 transmission profiles [*Gordley et al.*, 2009]. Our point-to-point precision is better than 1 m, so setting the altitude for one point effectively sets it for the whole profile. The CO_2 used to simulate the transmission is from the WACCM model output. The altitude registration for v1.022 is performed near 35 km, where the WACCM CO_2 has negligible uncertainty, so that does not contribute to altitude uncertainty. However, the forward model error will cause some uncertainty, but that is typically well under 50 m. The H_2O channel altitude uncertainty is primarily due to the uncertainty of the relative alignment of the H_2O channel with the sun sensor and the H_2O channel with the 4.3 μm CO_2 channel (i.e., channel 7). In this analysis, the uncertainty for altitude registration is assumed to be ~100 m at all altitudes. The corresponding error response varies from 1.5% (~0.12 ppmv) to 2.5% (0.04 ppmv) from lower to upper mesosphere.

[14] Line strength error was simulated by applying a 1.5% perturbation to each line strength value and the response by vmrs is found to be directly proportional by the same percentage at all altitudes. Air broadened half-width error was simulated by applying a 5% perturbation to each half-width value. The response is overall small, and especially above 65 km, it is negligible. Below 55 km, the error is about 1.0%–1.5% and mainly comes from the pressure broadening. Above 65 km, the Doppler broadening dominates. In the SOFIE retrieval, the Doppler line shapes are modeled to a high accuracy, and therefore the error responses are negligibly small (<0.1%).

[15] The forward model error presents the differences observed in off-line H_2O retrievals done with the rigorous line-by-line retrieval algorithm (Linepak) [*Gordley et al.*, 1994] and the fast, but accurate, Bandpak [*Marshall et al.*, 1994] algorithm that employs the emissivity growth approximation. This error response to the forward model actually represents a bias that can be corrected in future data versions. It is generally small in the middle atmosphere, which is <0.1 ppmv at nearly all listed altitudes except at 75 km it reaches 0.14 ppmv.

[16] The total systematic error by percentage is ~9%–16% at 85 km and above and decreases to ~3%–4% in the lower mesosphere; whereas by vmrs it is about ~0.2–0.3 ppmv at all listed altitudes indicating a weak dependence on altitude. By percentage the random error and the systematic error are comparable above 85 km but in the lower to middle mesosphere the systematic error dominates.

3. Data Sets Used in SOFIE H_2O Validation

3.1. ACE-FTS H_2O

[17] SCISAT-1 was launched into a 74° inclination 650 km circular orbit on 12 August 2003 and is still operating to date. The Atmospheric Chemistry Experiment Fourier Transform Spectrometer (ACE-FTS) on the SCISAT-1 is a high-resolution (0.02 cm^{-1}) infrared Fourier transform spectrometer (750–4400 cm^{-1} or 13.3–2.2 μm) that measures the vertical profiles of trace gases and temperature [*Bernath et al.*, 2005]. The instrument works in a solar occultation mode with the vertical sampling varying from 1.5 to 6.0 km. The H_2O retrieval utilizes 60 microwindows which fall in the 950–975 cm^{-1} (10.5–10.25 μm) and 1360–2000 cm^{-1} (7–5 μm) spectral ranges to retrieve profiles from 5 to 90 km altitude [*Carleer et al.*, 2008]. Version 2.2 of the ACE-FTS H_2O is used in this study. ACE-FTS H_2O single profile random error is given in the data files, which indicates a high precision that remains ~2%–4% up to ~80 km. ACE-FTS and SOFIE can only achieve limited spatial overlap in each season because the ACE-FTS sunset (or sunrise) latitudes change from one hemisphere to another, i.e., 85°N–65°S (or 65°N–80°S) every few weeks [*Bernath*, 2006], while the SOFIE sunset (or sunrise) measurement latitudes remain in one hemisphere and only occur in polar regions.

3.2. MLS/Aura H_2O

[18] The Microwave Limb Sounder (MLS) on the Aura satellite was launched on 15 July 2004 into a 98° inclination 705 km altitude, Sun-synchronous circular orbit. The MLS line of sight is in the forward along-track direction of the Aura spacecraft. The Earth's limb is scanned from the surface to 90 km every 26.6 s giving 240 scans per orbit spaced at 1.5° intervals (165 km) with a total of 3500 vertical profiles per day and nearly global latitude coverage from 82°S to 82°N [*Lambert et al.*, 2007]. MLS measurements are made in five spectral bands, at 118 GHz, 190 GHz, 240 GHz, 640 GHz, and 2.5 THz [*Waters et al.*, 2006; *Livesey et al.*, 2006]. The standard H_2O product used here is

taken from the 190 GHz band retrieval. The useful vertical range of v2.2 MLS H_2O is 316–0.002 hPa. The MLS H_2O vertical resolution is ~3–6 km at pressures higher than 0.22 hPa (~60 km) with a single-profile precision of ~4%–5%. At pressures lower than 0.1 hPa (~66 km) the vertical resolution degrades to 14–16 km and the precision worsens to >10%. The estimated systematic errors vary from 4% to 34% from the upper stratosphere to the lower thermosphere [*Livesey et al.*, 2007; *Lambert et al.*, 2007]. Three data quality indices are applied prior to the use of MLS H_2O data, i.e., only profiles with positive precision values, a status field of even numbers, and a quality field greater than 0.9 are used in the comparisons shown later.

3.3. HALOE Vpmc Data

[19] The Halogen Occultation Experiment (HALOE, 1991–2005) [*Russell et al.*, 1993] made measurements of temperature versus pressure, many trace gases (HF, HCI, CH_4, NO, NO_2, H_2O, O_3), and aerosols that are of great importance in the middle atmosphere. The overall vertical resolution of HALOE NO_2, H_2O, and O_3 is ~2 km. Water vapor from the latest public release version 19, however, is not valid in the polar summer mesosphere due to known PMC contamination of the signals. To resolve this issue a special processing algorithm (Vpmc) was developed to remove the PMC absorption in the gas channels [*McHugh et al.*, 2003]. In the vertical range 80–85 km the total estimated systematic error for Vpmc H_2O is about ~18%. In this study Vpmc1.1 H_2O is used to make qualitative comparisons with SOFIE H_2O in the upper mesosphere.

4. SOFIE H_2O Comparisons With Correlative Data Sets

4.1. Strategies

[20] The basic approach for validation is to examine the statistical moments of the near-coincident pairs between SOFIE and the correlative data sets. Within a given time interval (e.g., a few hours) the pair of profiles with the closest geographic distance is selected as the coincidence. Criteria for temporal and spatial coincidences can vary with the correlative data sets. For example, SOFIE and ACE-FTS can achieve a near-coincident state only during a very limited period in any given season based on the SCISAT-1 orbital information (http://www.ace.uwaterloo.ca/mission_orbit.html) [*Bernath*, 2006]. To obtain more than just a few coincidences, we used a wider latitude range for the ACE-FTS comparisons, i.e., ±5°, and correspondingly the longitude and time ranges are set to ±20° and 4 h, respectively. SOFIE and MLS can achieve much closer spatial coincidence owing to the denser spatial coverage of MLS data points. A more confined spatial coincidence box, i.e., ±10° in longitude and ±2° in latitude, is set for SOFIE and MLS, but the time interval is still set to 4 h as it is roughly the required span to find coincidences in the NH summer.

[21] Vertical interpolation and smoothing procedures are applied prior to the statistical analysis to ensure that both SOFIE and the correlative data sets are placed on common grids and their vertical resolutions are better matched. The vertical profiles from the two data sets are compared on a pressure coordinate, and the common grids are generated based on the equal-spacing of the log-pressure values. Both FFT (Fast Fourier Transform) low-pass smoothing and averaging kernel (AK) smoothing are used [e.g., *Froidevaux et al.*, 2008]. FFT smoothing is an efficient approach to remove the smaller scale fluctuations when AKs are not provided. However, for FFT smoothing to be conveniently applied, we must ensure that the correlative data set has a near-constant vertical spacing throughout the altitude range of the interest. ACE-FTS H_2O shows a near-constant vertical spacing of 5–6 km above 35 km therefore a FFT smoothing with a half sinusoidal wavelength of 6 km is applied to each SOFIE H_2O profile prior to the comparisons. In the SOFIE versus MLS H_2O comparisons AK smoothing is used. This approach better suits the situation since the MLS H_2O vertical resolution varies significantly over its whole vertical range. MLS H_2O AKs are given as a 47×47 square matrix spanning the pressure levels from 1000 to 10^{-5} hPa. We use the formula $x_{\text{smooth}} = \hat{x}_a + A \cdot (x_{\text{interp}} - \hat{x}_a)$ to apply smoothing to any given SOFIE profile, where $\hat{x}_a$ is the MLS a priori profile in polar latitudes, A is the MLS AK matrix, and x_{interp} is the SOFIE profile linearly interpolated onto the a priori vertical grid, which is approximately ~3 km equally spaced [e.g., *Rodgers and Connor*, 2003].

[22] The variable of interest in the validation is the difference of SOFIE and the correlative data H_2O vmrs at given log-pressure levels. The statistical moments used are the mean and the 1-σ standard deviation (STD) of the differences in percent. The standard error of the mean (SEM) is defined as the STD divided by the square root of the number of coincidences. The SEM goes to zero asymptotically when there are an increasing number of coincidences, indicating a mean difference with high statistical significance. The combined random error shown in the following comparisons refers to the root sum square of the random errors provided by the individual data sets.

[23] The analyses are performed for the NH and SH separately and are divided into three seasonal groups, summer, winter, and spring/fall combined. The summer months include June, July, and August (JJA) in the NH, and December, January, and February (DJF) in the SH, and it is opposite for winter. The grouping scheme is based on the previous knowledge that summer is the season during which the mesospheric H_2O is enhanced, resulting in a qualitatively different vertical distribution from that of any other season. Although winter H_2O vertical distribution does not differ significantly from that in spring or fall, it is treated separately because there is possibly a larger random variability in winter than in spring/fall owing to the difference in the eddy activity.

4.2. Results of Comparisons

[24] All of the coincidences between SOFIE and ACE-FTS H_2O profiles in the 2007–2008 NH are used to calculate the statistics shown in Figure 3. In NH summer the mean profiles show excellent agreement between 60 and 75 km (0.3–0.02 hPa), and correspondingly the mean percentage difference indicates a near-perfect agreement in this vertical range. The STD of the differences shows a small degree of scatter (~2%–5%) that is close to but slightly exceeding the combined precision. In the middle to upper mesosphere (>75 km) the agreement is not as good, with the absolute (or mean percent) difference varying between −0.7 and 1.0 ppmv (or between −15% and 15%). This difference

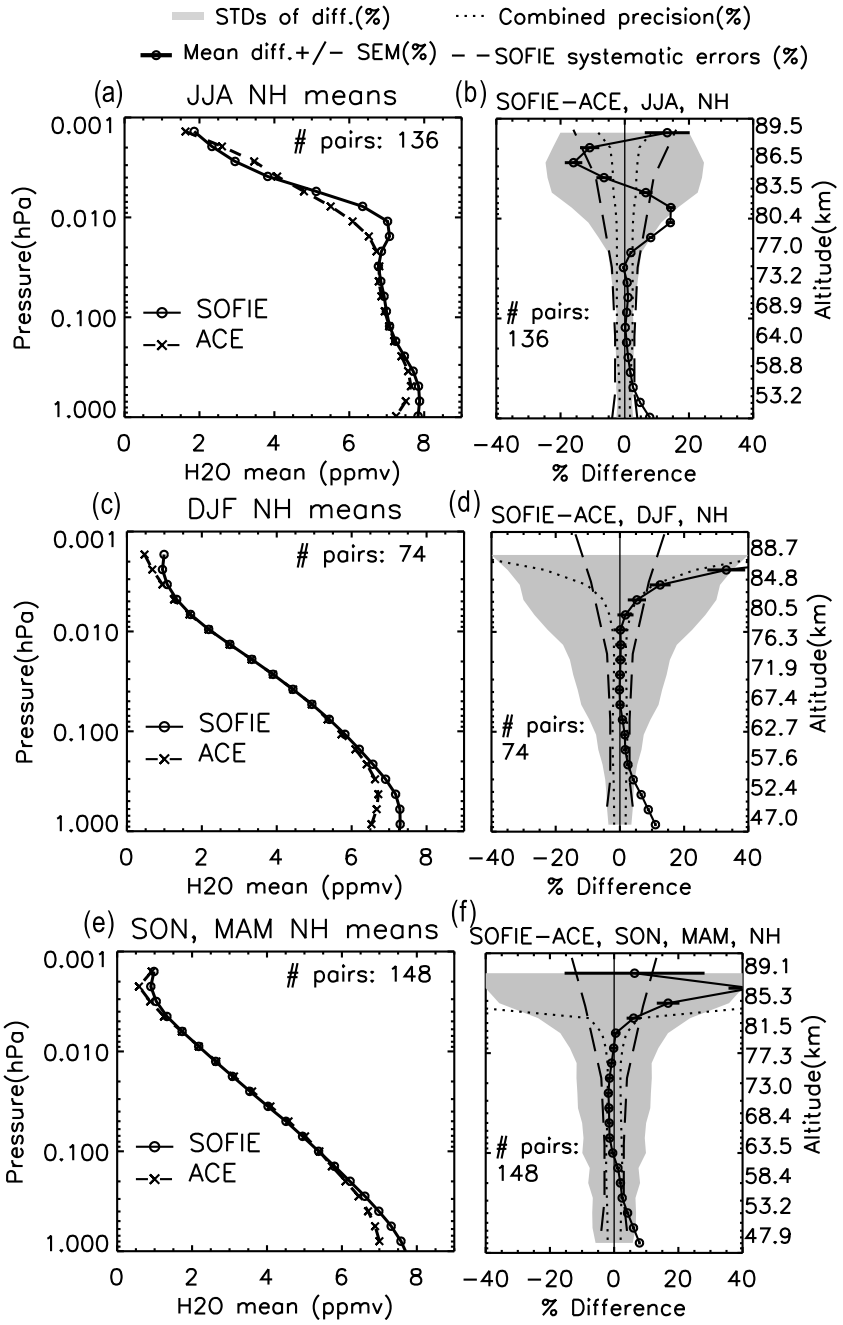

Figure 3. SOFIE versus ACE H_2O comparisons in the NH (a and b) summer (June, July, and August), (c and d) winter (December, January, and February), and (e and f) the fall and spring combined. All coincidences from May 2007 to July 2008 are used. (left) The mean profiles of the two data sets; (right) statistics of the differences of the coincident pairs. Legends at the top are for the right frames. The altitude values indicated on the right-hand side vertical axes are based on the SOFIE altitude and pressure, as is also the case in Figures 4–6.

is due to a notable enhanced layer in the SOFIE H_2O mean profile at ~80 km that is not present in the corresponding ACE-FTS mean profile, together with a more rapid decrease of SOFIE H_2O above ~80 km. The enhanced layer in the SOFIE mean profile is clearly visible because it appears in a majority of the SOFIE profiles in polar summer. Further investigation (not shown) indicates that a small percentage of ACE-FTS profiles in polar summer also exhibit such a feature with a comparable magnitude but after averaging many profiles it is no longer discernable. At ~80 km the mean percentage difference exceeds the SOFIE systematic error by ~10%, confirming the significant difference between ACE-FTS and SOFIE in this range. The STD in the upper mesosphere (>83 km) is ~20%–22%, far exceeding the combined precision. In the polar summer the gravity wave breaking at ~80–90 km can lead to an eddy turbulent effect;

also the appearance of PMCs, which is highly variable, affects the H_2O budget significantly. Both can result in a larger variability.

[25] The mean profiles in winter and spring/fall (Figures 3c and 3e) show near-perfect agreement in the vertical range ~60–80 km but above ~80 km the two data sets show biases that exceed 40%. The large SEM values suggest relatively poor reliability of the mean percentage difference, especially above ~86 km. The winter STD is systematically larger than the summer STD, especially in the lower to middle mesosphere. The summer STD is small because the small scale disturbances in summer profiles are removed when smoothing is applied. In winter, on the other hand, not only can a broader spectrum (i.e., larger scales) of gravity waves penetrate into the mesosphere, but also they break at lower altitudes (i.e., ~60–80 km) [*Garcia and Solomon*, 1985]. These larger-scale disturbances remain even after the smoothing is applied, which explains the larger winter STD. The spring/fall STD is overall smaller than during winter but still its magnitude is closer to the winter case. This is because the typical spring or fall is usually short (~1 month), during which H_2O experiences a rapid transition between summer and winter states, while for the remaining time the circulation more or less resembles the winter condition. At last it is worth pointing out that in the upper stratosphere to stratopause region for all seasons SOFIE H_2O is biased high by ~0.7 ppmv (~7%–10%) relative to ACE-FTS H_2O.

[26] In Figure 4 a similar set of plots are shown for the SH comparisons. The comparisons for summer (top) indicate that SOFIE H_2O is consistently lower than ACE-FTS H_2O by ~0.5–0.7 ppmv (~10–20%) at nearly all altitudes except at ~80–83 km where the two data sets agree better. The closer agreement near 80 km appears to be related to H_2O enhancement layer due to PMC sublimation observed by SOFIE although the magnitude is much smaller than its NH counterpart. The nearly uniform bias is particularly distinct in winter and spring/fall (Figures 4c and 4e). It is worth mentioning that despite the significant magnitude of the bias, the vertical slopes of the two data sets agree very well in the mesosphere.

[27] SOFIE and MLS H_2O comparisons in the NH are shown in Figure 5, using the coincidences found in 2007–2009. We have applied the MLS averaging kernels (AKs) to smooth the SOFIE H_2O to better match the MLS vertical resolution. In summer in the vertical range ~60–82 km (~0.2–0.006 hPa) the mean percentage differences are within 0%–5%, indicating excellent agreement. However a structure at ~66 km that indicates a high SOFIE bias should be noted. A separate investigation (not shown) suggests that this structure is a reflection of the narrower SOFIE enhancement layer at ~80 km that is projected into a broader range when the AK smoothing was applied. The mean profiles in winter and spring/fall also show overall very good agreement between SOFIE and MLS below ~83 km, with an absolute difference of 0–0.5 ppmv and a mean percentage difference of −5%–10%. In all seasons of NH comparisons the mean percentage difference stays within the combined systematic error throughout the mesosphere, confirming overall reasonable agreement between SOFIE and MLS. In the upper stratosphere to stratopause region (~45–55 km) SOFIE H_2O is greater than MLS H_2O by ~6%–10%, which is very similar to the ACE-FTS comparisons. In both comparisons, the mean percentage difference exceeds the SOFIE systematic error or combined systematic error by ~1%–5%, suggesting a robust high bias of SOFIE H_2O in this vertical range.

[28] In the SH (Figure 6), SOFIE H_2O is consistently lower than MLS H_2O throughout the whole vertical range and for all seasons, with the difference in summer especially large. The large bias in summer, characterized by an absolute difference of ~1–2 ppmv and a mean percentage difference of >15%, is related to an unusually steep vertical slope of MLS H_2O in the altitude range ~60–82 km. Previously ACE-FTS comparisons also show consistent low bias of SOFIE H_2O in the SH, but the magnitude in summer is less pronounced than with MLS H_2O. In winter and spring/fall, the vertical slopes of MLS H_2O are also different from those of SOFIE H_2O, causing the larger differences above ~80 km and around ~63–65 km. In the SH throughout the mesosphere the mean percentage difference exceeds the combined systematic error by 10% or more, which suggests that the two data sets are significantly biased.

5. Other Validations: SOFIE Summer Mesospheric H_2O Intraseasonal Variation

5.1. Observed H_2O in the Upper Stratosphere and Mesosphere

[29] Altitude versus time (days from solstice or DFS) cross sections of the SOFIE daily zonal mean H_2O are shown in Figure 7. It should be noted that the SOFIE latitude increases significantly from early to late summer (white curves). As a result the latitude dependence of H_2O could be an important consideration. However, the polar summer (north/south of 65°) H_2O latitudinal dependence is overall weak (not shown), and therefore the H_2O seasonal variation at SOFIE latitudes is representative of the averaged state of the entire polar summer region. The time period is from May to October for the NH and November to April for the SH, respectively. It is noted that in the NH (or SH) the H_2O increases throughout May to mid-August (or November to mid-February) and rapidly decreases in September (or March). In the upper mesosphere in both the NH and SH there is a region with a strong vertical gradient (~83–90 km) that separates the high and low H_2O vmrs. This vertical distribution of the H_2O contours in the mesosphere is shaped primarily by the competing effect of photochemical dissociation and the vertical transport, although in the vertical range 55–65 km a very small fraction of H_2O vmr may still come from the CH_4 oxidation in the polar summer. The CH_4 vmr level in the vertical range 55–65 km is ~0.1 ppmv. According to a well-established theory, the intensity of upwelling in the summer solstice increases with height [e.g., *Garcia and Solomon*, 1985; *McIntyre*, 1989]. Such a vertical distribution of the upwelling will result in the divergence of the H_2O contours in the lower to middle mesosphere but convergence in the upper mesosphere. Another striking feature in the NH is the existence of a sequence of "small cells" just below the high gradient region around 80 km that indicates a layer of enhanced H_2O. This layer was identified as a PMC induced layer by *Summers et al.* [2001]. It is also noted from Figure 7 that this layer is pronounced only after the summer solstice when H_2O vmr has increased significantly and the PMCs are seasonally strong. Although this is

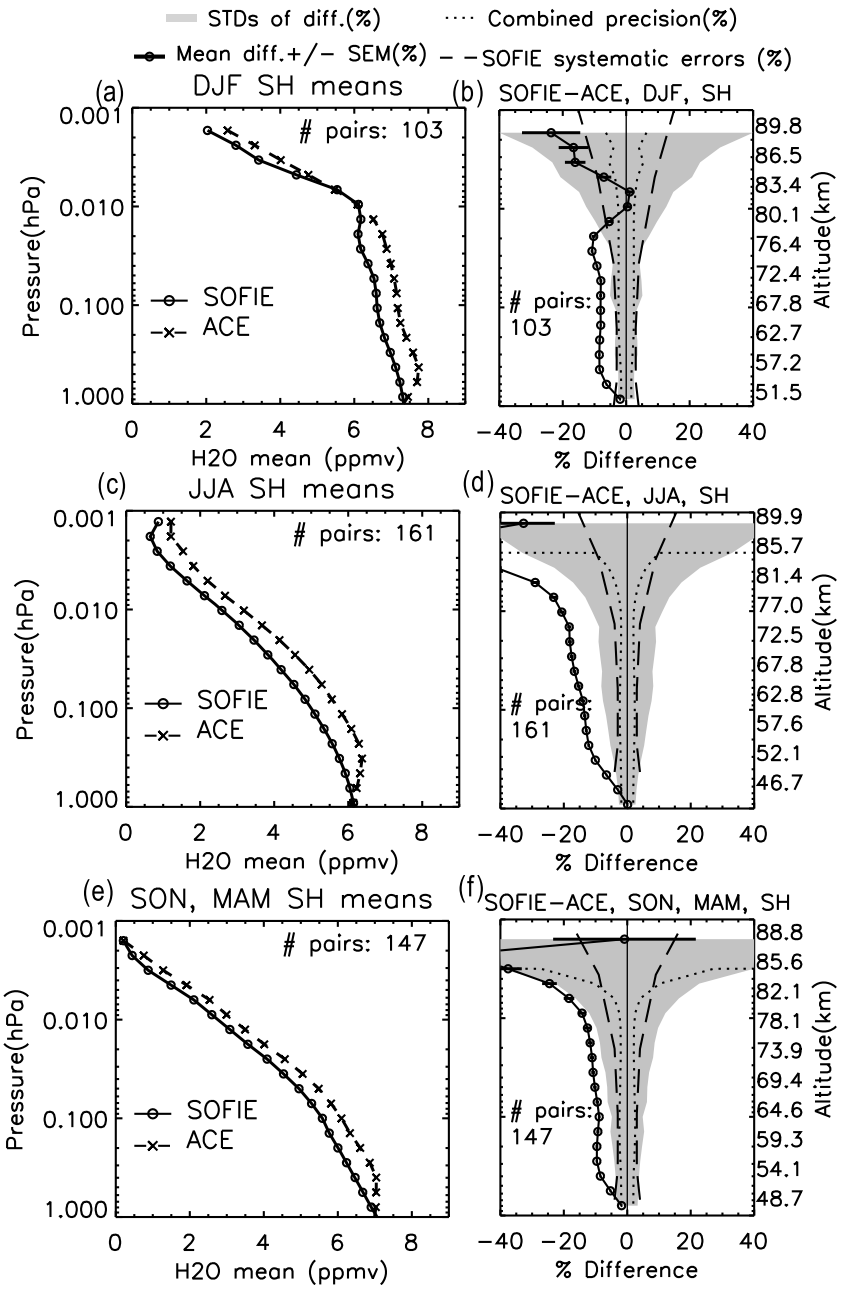

Figure 4. Same as in Figure 3, except for SH comparisons. December, January, and February are chosen as the SH summer months.

an unequivocally clear and persistent feature in SOFIE H_2O, its magnitude is much less prominent than in the HALOE analysis shown by *Summers et al.* [2001]. In Figure 8 we show the comparisons of SOFIE H_2O in 2008 and HALOE Vpmc H_2O in 1996 in the upper mesosphere. For each hemisphere, two periods of the PMC season are chosen during which HALOE and SOFIE latitudes are very close. For both hemispheres, we note that in early summer the enhancement layer in HALOE H_2O is prominent while in SOFIE it is barely discernible. In fact, in the SH the enhancement layer has not yet developed in December. In late summer both data sets show the strongest enhancement layer. In SOFIE, the enhancement layer stands out from the background by ~1.0 ppmv, while in HALOE it reaches ~3.0 ppmv. For both data sets, the SH enhancement layer is weaker than the NH counterpart but it is more so in SOFIE. It should be noted that HALOE H_2O is much more noisy with a random error of ~98% [see, e.g., *Wrotny and Russell*, 2006], which makes the averaging method an important consideration in determining the peak value. For example, *McHugh et al.* [2003] performed a 10 day time bin and multiple-year average and obtained a seasonal maximum of ~8.5–9.0 ppmv, which is slightly smaller than the values shown in Figure 8. While HALOE does observe a more prominent H_2O enhancement layer than SOFIE, the results are less reliable. Incomplete removal of the PMC signal causes the HALOE H_2O upper altitude peak to be exaggerated at times and therefore it is not a good indicator

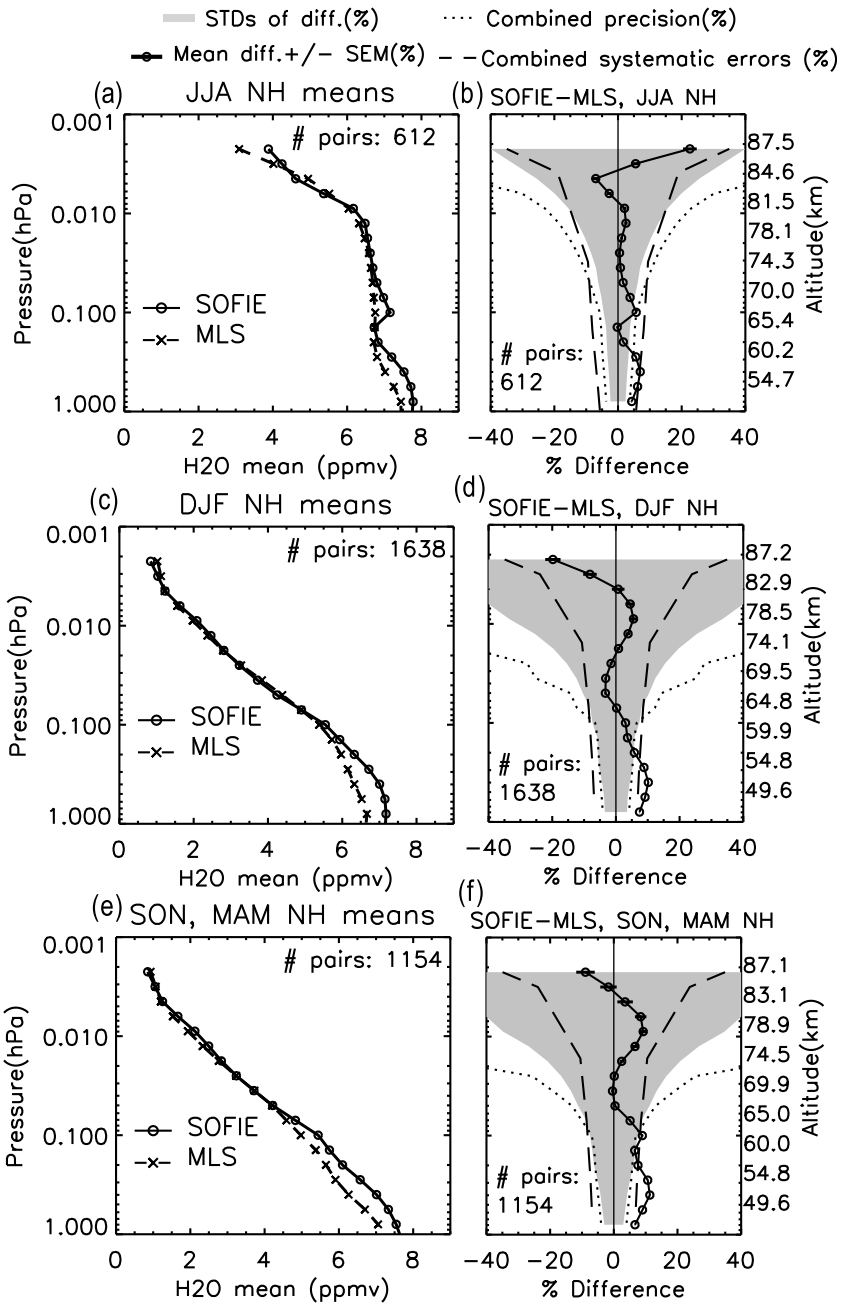

Figure 5. SOFIE versus MLS comparisons in the NH, shown in the same format as in Figure 3. All coincidences from June 2007 to February 2009 are used.

of the magnitude of the PMC induced maximum in H_2O. This difference between the two data sets represents a long existing discrepancy between satellite observations and the results from some photochemical models [*Summers et al.*, 2001; *Stevens et al.*, 2001] or PMC models [e.g., *Rapp et al.*, 2002; *von Zahn and Berger*, 2003]. The model results often suggest a more prominent enhancement layer than most satellite data sets have shown. However, the final conclusion on this point remains unclear. For example, a PMC model by *Jensen and Thomas* [1988] indicates that cloud sublimation produces a H_2O enhancement layer of ~0.5–1.0 ppmv above the background values, which agrees with the SOFIE observations.

[30] Even though the main focus of the SOFIE mission is in the mesosphere, the upper stratosphere is also of great scientific interest especially for H_2O since it is the source region of the summer mesospheric H_2O. The high H_2O mixing ratio levels in the upper stratosphere to stratopause region come mostly from CH_4 oxidation, characterized by a year-round H_2O peak at ~45–55 km. However, the magnitude of the peak shows drastic seasonal variation. Figure 7 has shown that the peak is increasingly strengthened throughout summer and fall for both hemispheres. Furthermore, the orientation of the peak zone exhibits descent from late August to October for NH or February to April for SH. Figure 9 shows the altitude versus time cross section of

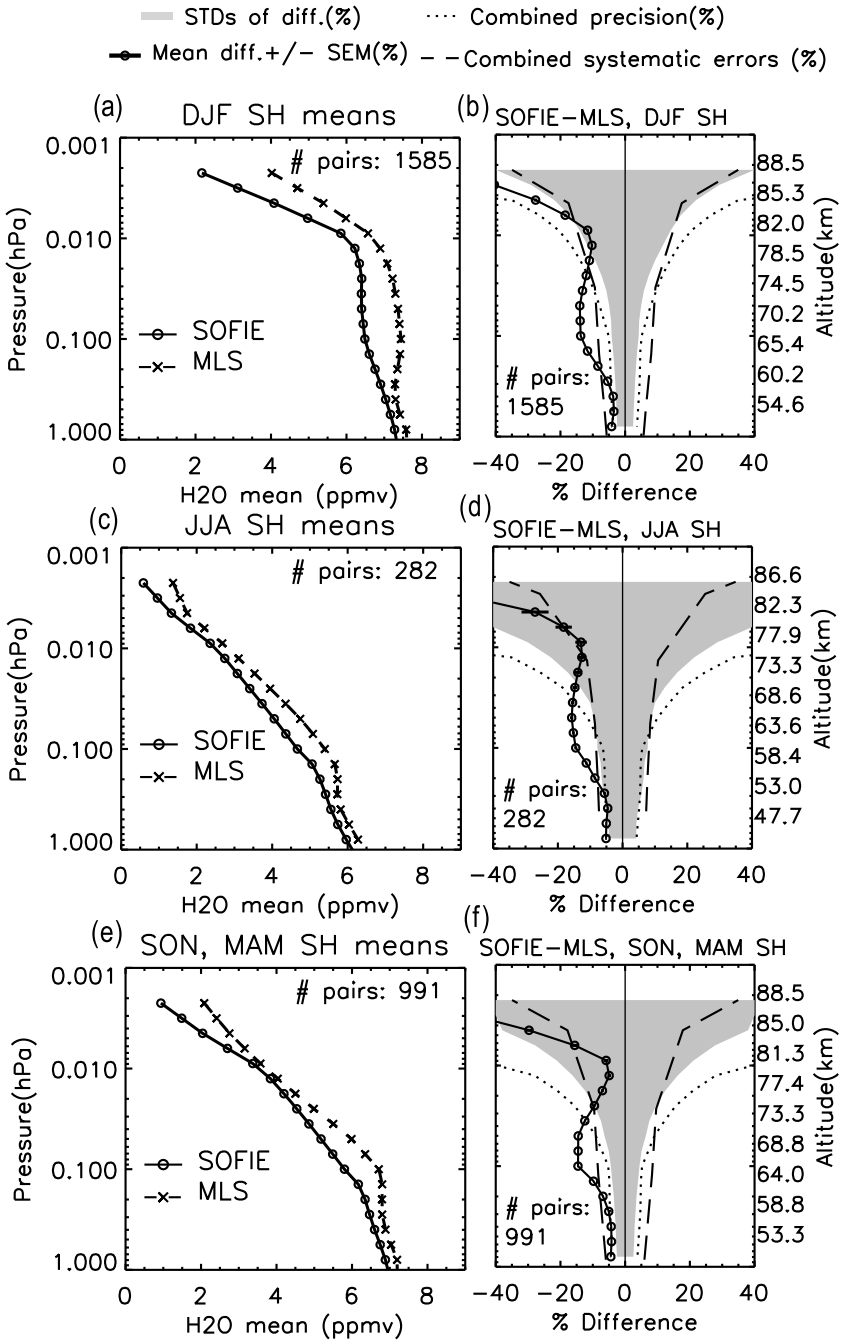

Figure 6. Same as in Figure 5, except for SH comparisons.

SOFIE daily mean CH_4 in the upper stratosphere and lower mesosphere through late summer and fall. Methane was retrieved from SOFIE channel 6 (strong) band 11 (3.384 μm) signals. Since the wavelength is very close to the PMC channel (3.064 and 3.186 μm), the signals in the upper mesosphere is contaminated. The vertical range of the v1.022 CH_4 retrieval is 20–70 km. We examine the same vertical ranges (45–55 km) in Figures 7 and 9 and note that the descending high H_2O vmrs are accompanied by a similar descent of low CH_4 vmrs. This is not surprising since in the upper stratosphere to lower mesosphere (~30–60 km) the potential H_2O ($H_2O + 2CH_4$) is expected to be approximately conserved [e.g., *Harries et al.*, 1996; *Nassar et al.*, 2005]. However, the particularly strong CH_4 conversion in fall around the stratopause region is noteworthy and needs interpretation. Comparing 2007 and 2008, we find stronger CH_4 depletion in 2008 which supports the slightly wetter condition in 2008 as is shown in Figure 7. As for the hemispheric difference, SOFIE CH_4 indicates slightly stronger depletion in the SH than in the NH in both years, which contradicts a drier SH shown in the SOFIE H_2O from late summer to early fall in the altitude range 45–60 km.

[31] Figure 10 shows an altitude versus time cross section of MLS H_2O. The profiles are averaged daily within a ±2.5°

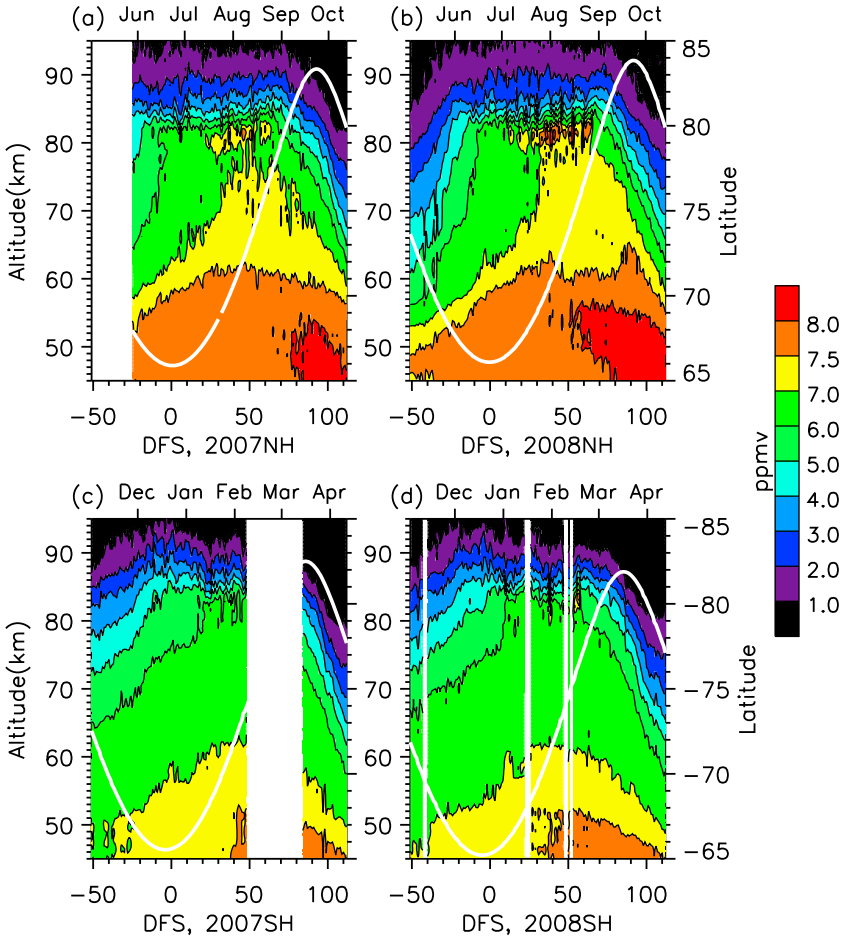

Figure 7. Altitude versus time cross sections of SOFIE daily zonal mean H_2O throughout summer and fall. The horizontal axis is days from summer solstice. The white curve represents the seasonal variation of the daily mean SOFIE latitudes. The month names are marked in the beginning of each month.

latitude range centered on the SOFIE latitudes. MLS H_2O is presented on altitude grids by matching the pressure levels between MLS and SOFIE and then applying the SOFIE altitude registration. Some major features in Figure 10 agree well with SOFIE H_2O, such as the high gradient versus low gradient regions above and below 83 km; a persistent increase of mesospheric H_2O until late August, a rapid decrease in September and the descent of the upper stratospheric peak zone. On the other hand, some differences should be noted. Although there appears to be a layer of enhanced H_2O in the upper mesosphere, the MLS H_2O exhibits a much broader vertical feature extending downward to ~65 km. The related issue has been discussed in the profile comparisons (see section 4.2) when a similar broad layer forms as SOFIE H_2O is smoothed by MLS AKs. A coarser resolution is definitely associated with the broadening effect. The most important disagreement between SOFIE and MLS lies on the hemispheric difference of the summer H_2O vmrs. SOFIE H_2O shows a persistently drier SH in the vertical range ~55–83 km after summer solstice, with an average difference of ~0.5–0.7 ppmv. In the same vertical range and time period MLS H_2O indicates a wetter SH prior to 35 DFS, with an average difference of ~0.2–0.5 ppmv. After this time the NH and SH vmrs grew extremely close to each other. It is worth pointing out that ACE-FTS H_2O also shows a slightly wetter SH (~0.2 ppmv) in July versus January when polar summer profiles were available, which basically supports the MLS observations.

5.2. H_2O Isopleth Slopes as an Indicator of the Polar Summer Upwelling

[32] In the polar summer mesosphere, gravity waves break at and above PMC altitudes (~80–90 km) and result in a wave drag force that drives the residual circulation (i.e., meridional component $\overline{v}^*$ and vertical component $\overline{w}^*$) throughout the mesosphere [e.g., *McIntyre*, 1989; *Garcia and Solomon*, 1985]. In the transformed Eulerian mean (TEM) framework the constituent variation is balanced by the sum of several terms, i.e., photochemical production or destruction, advective transport by the residual circulation, and eddy diffusion due to breaking gravity waves [e.g., *Garcia and Solomon*, 1985; *Andrews et al.*, 1987]. In the polar summer mesosphere, there is no other known chemical source of H_2O except that in a narrow vertical range from ~50 to 60 km, methane oxidation may still contribute a small fraction of the H_2O present [e.g., *Harries et al.*, 1996]. In addition, below the wave breaking levels the vertical transport by eddy diffusion and H_2O photodissociation

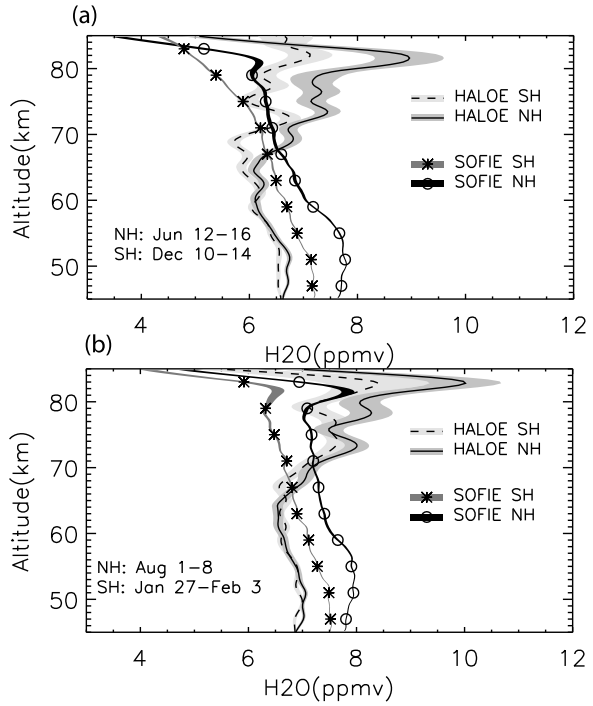

Figure 8. Comparisons of HALOE and SOFIE H_2O in the mesosphere during the PMC season when an enhanced H_2O layer is observed in both data sets. HALOE Vpmc 1.1 H_2O in 1996 and v1.022 SOFIE H_2O in 2008 are used. The two time periods are chosen when the two data sets have very similar latitude coverage. The shaded range is the mean H_2O profile plus and minus the SEM.

combined is small in magnitude compared to the vertical transport by the residual circulation. The above conditions suggest that H_2O in the lower to middle mesosphere can be treated as a tracer for the residual circulation [e.g., *Brasseur and Solomon*, 2005].

[33] The residual circulation for all four seasons has been modeled or diagnostically calculated in a series of previous studies [*Garcia and Solomon*, 1985; *Rosenfield et al.*, 1987; *Huang and Smith*, 1991; *Hoppel et al.*, 2008]. Nevertheless, a continuous intraseasonal variation of the circulation on a daily basis was not shown in these studies. In this paper SOFIE H_2O isopleth slopes serve as direct evidence to reflect the intraseasonal variation of upwelling air motion ($\overline{w}^*$) in the polar summer mesosphere since the general summer H_2O enhancement is primarily attributed to the upwelling. For the isopleth slopes to maximally reflect the upwelling, the H_2O should be known continuously in time and space. SOFIE H_2O has high vertical resolution (~2 km) and year-round polar coverage; therefore, it is an excellent candidate for this research purpose.

[34] Figure 11 shows the altitude versus time behavior of selected isopleths of H_2O. Each of the lines in Figure 11 represents a different isopleth, shown at intervals of 0.2 ppmv. The color coding along each line represents the daily mean rate of change of the altitude of the isopleth, in cm s^{-1}. A 10 day smoothing was applied to the initially obtained isopleths prior to calculating the slopes to remove the excessive oscillations. The thick blue curves are the time series of the mean slopes in the altitude range 70–80 km, which is roughly the peak zone of positive slopes throughout the summer. Data for year 2008 in both hemispheres are analyzed to represent the cases for the NH and SH, and the slopes of SOFIE and MLS are shown in the left and right, respectively. For MLS we are only able to use those

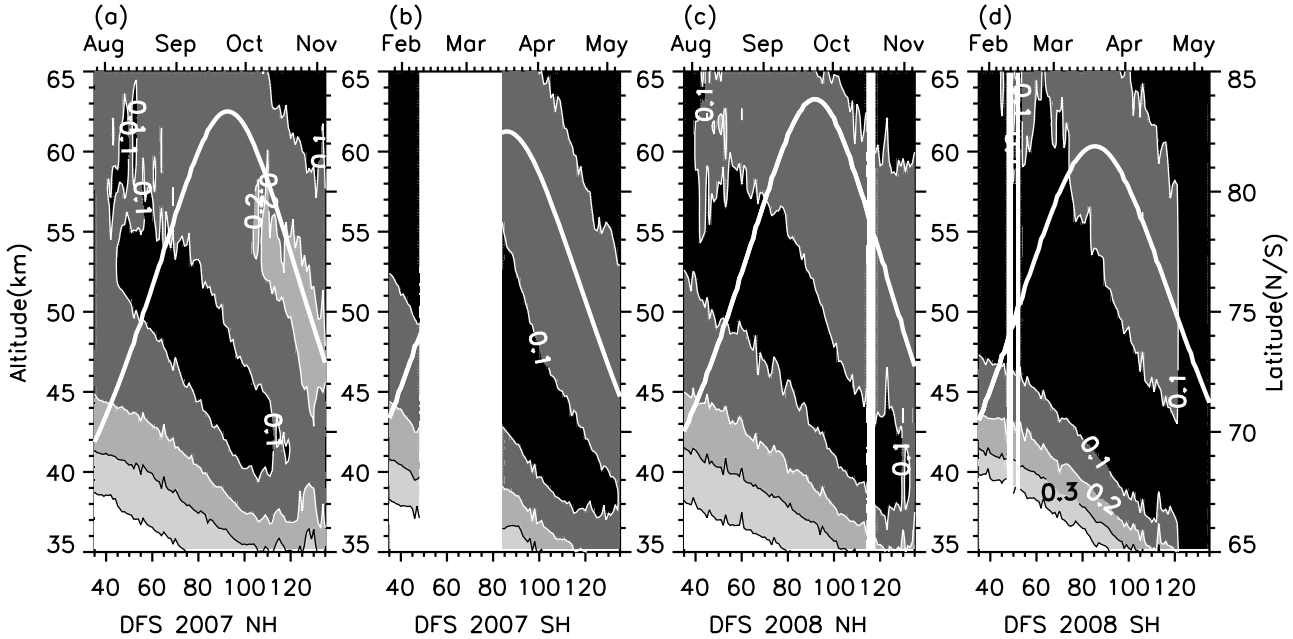

Figure 9. Altitude versus time cross sections of SOFIE daily zonal mean CH_4 in fall. The horizontal axis is days from summer solstice. The contour values are 0.1, 0.2, 0.3, and 0.4 ppmv. The thick white curve represents the seasonal variation of the daily mean SOFIE latitudes.

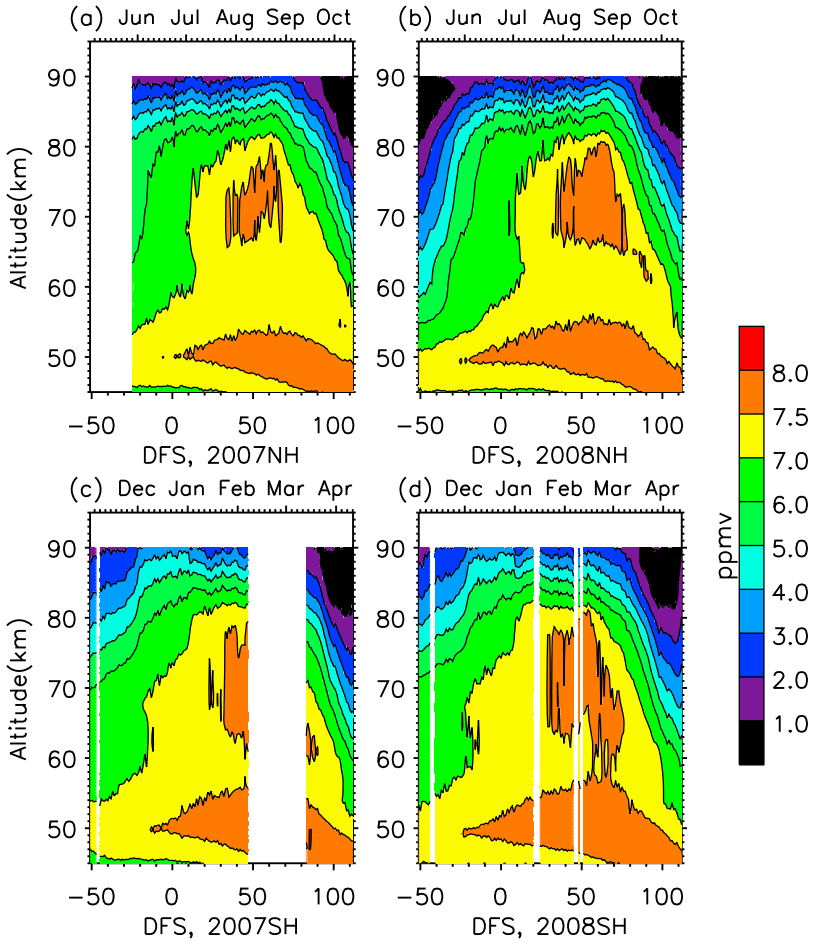

Figure 10. Altitude versus time cross sections of MLS H_2O profiles averaged over the SOFIE latitude ±2.5° range daily.

isopleths that are not strongly contaminated by the broad enhancement layer; therefore, in July and August MLS isopleths are not usable below 80 km.

[35] SOFIE H_2O slopes in the NH summer (Figure 11a) indicate that from mid-May to mid-June, the positive slopes are overall the largest, presenting two maxima in each month, with the larger maximum (>1.4 cm/s) reached in June. In the vertical dimension the peak value occurs at ~77 km, which is around 2–3 km lower than the peak altitude of the upwelling obtained by *Huang and Smith* [1991] using the climatological data. The maximum isopleth slope is slightly smaller but is very close to the upwelling in a similar latitude range (66°N–70°N) shown by *Huang and Smith* [1991]. This magnitude is however halved from the model result shown by *Garcia and Solomon* [1985]. The daily peak value of the positive slope decreases significantly in July and August. Especially in August, below 65 km the H_2O slopes start to turn negative, indicating that the vertical range of the upwelling is gradually confined to the middle mesosphere and above. The counterpart in the MLS analysis (Figure 11b) agrees with the SOFIE result by showing two maxima in May and June with slightly larger magnitudes. The 2–3 km lower peak altitude of the isopleth slopes is expected, because even if a large upwelling persists in the upper mesosphere, which is very likely the case, the isopleth slopes are unable to reflect this due to a much stronger photodissociation of H_2O at this height. The overall larger isopleth slope in June indicates that a strong upwelling may have persisted throughout the mesosphere, resulting in systematic upward transport of H_2O; while in July and August the upwelling is weakened in the lower to middle mesosphere.

[36] In SH summer shown in Figures 11c and 11d, both SOFIE and MLS analyses indicate much weaker positive slopes (<0.5 cm/s) than in the NH, and there are two maxima reached in early December and early January, respectively. Again MLS slopes are larger than SOFIE slopes. The SOFIE slopes in January are the largest and they occur in a broader altitude range of the mesosphere than in December, and meanwhile the centroid height of the H_2O high gradient region is notably decreased in January. This may suggest an increase of the gravity wave drag in January compared to the earlier season, resulting in the downward shift of the wave breaking altitudes and mesopause height, and a larger upwelling in the lower to middle mesosphere [*Garcia*, 1989].

[37] In September in the NH and in March in the SH, the slopes are persistently negative with a magnitude of ~0.5–0.8 cm/s regardless of the data set or hemisphere. Such a slope again is similar to the result of *Huang and Smith* [1991] but is halved from the downwelling magnitude shown by *Garcia and Solomon* [1985] in the same latitude range (>80°). It is also worth pointing out that during the equinox period the eddy diffusion is weakened so the

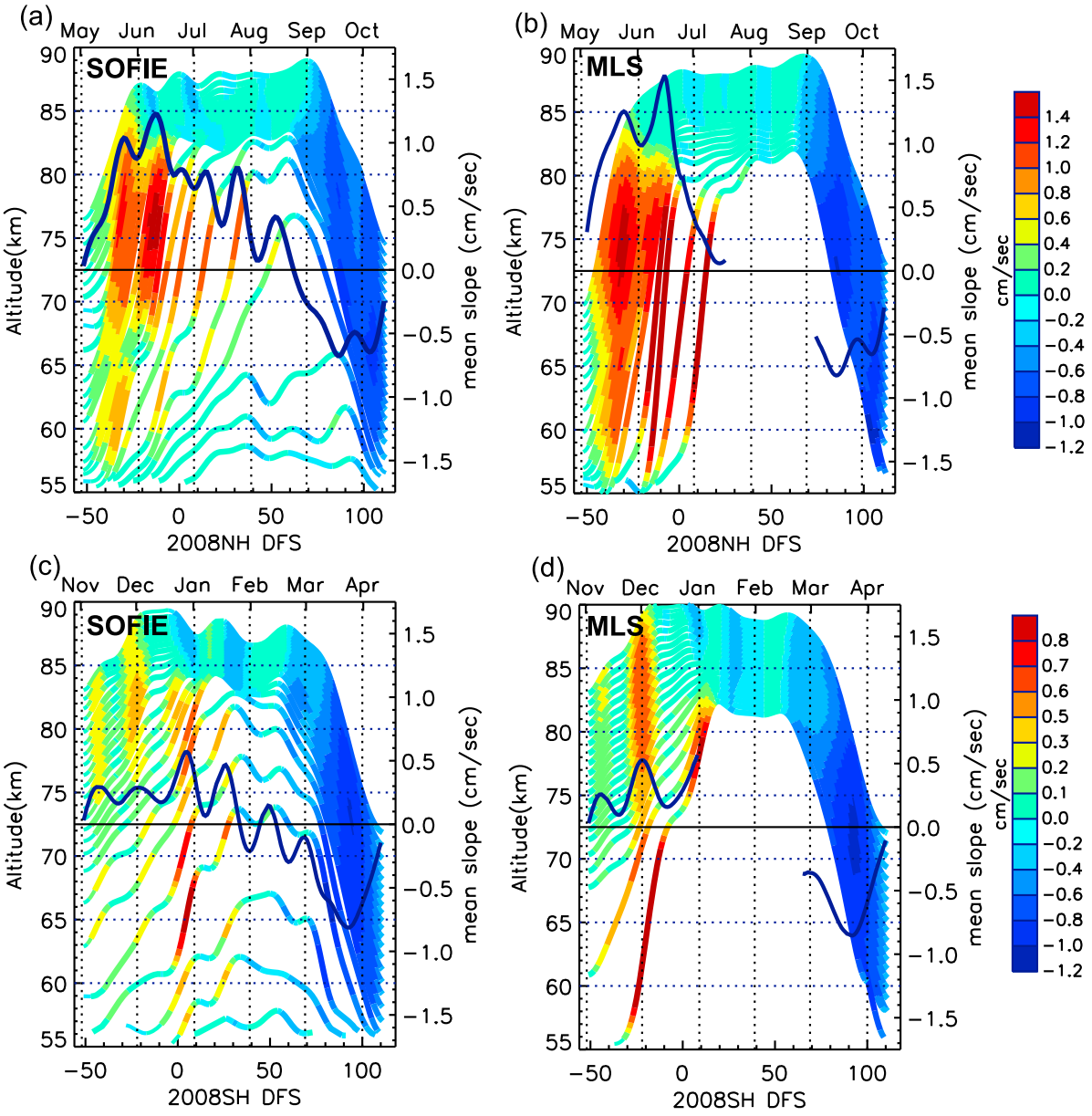

Figure 11. A set of mesospheric H_2O isopleths (at intervals of 0.2 ppmv) with the color representing the daily mean slopes (cm/s). The SOFIE and MLS analyses are shown in the left and right, respectively. We only include those open isopleths which particularly reflect the mesospheric upwelling effect on the H_2O redistribution. In this regard the MLS isopleths with H_2O vmr >7.0 ppmv are avoided. To further clarify the temporal variation of the slopes, the time series of the vertical average in the altitude range 70–80 km (dark blue curve) is superimposed.

photochemical dissociation probably takes stronger role than during the summer. A future modeling study that simulates the competition between the chemical and the dynamical effects would provide further interpretation of the H_2O distribution observed by SOFIE.

5.3. H_2O vmrs at the PMC and Mesopause Heights

[38] Figures 12a and 12b show the 2007 NH summer intraseasonal variation of daily mean H_2O in the upper mesosphere from both SOFIE and MLS, along with the daily mean SOFIE PMC and mesopause heights. The SOFIE PMC height for a given event is defined as the height where the maximum ice mass density occurs when clouds are detected. The ice mass density (ng/m^3) is retrieved using the SOFIE 3.064 μm extinction profiles [*Hervig et al.*, 2009]. It is clear, especially for SOFIE, that the H_2O high gradient region above ~80 km follows similar temporal variations as those for the mesopause and PMC heights on a range of time scales from a few days to seasonal scales. However, there is a distinct two-stage evolution in the relationship between the mesopause height (or PMC height) and the high-gradient region. In the beginning of the season both the PMC and mesopause heights coincide with the H_2O isopleths of lower vmr values, i.e., ~2.5 ppmv for mesopause height

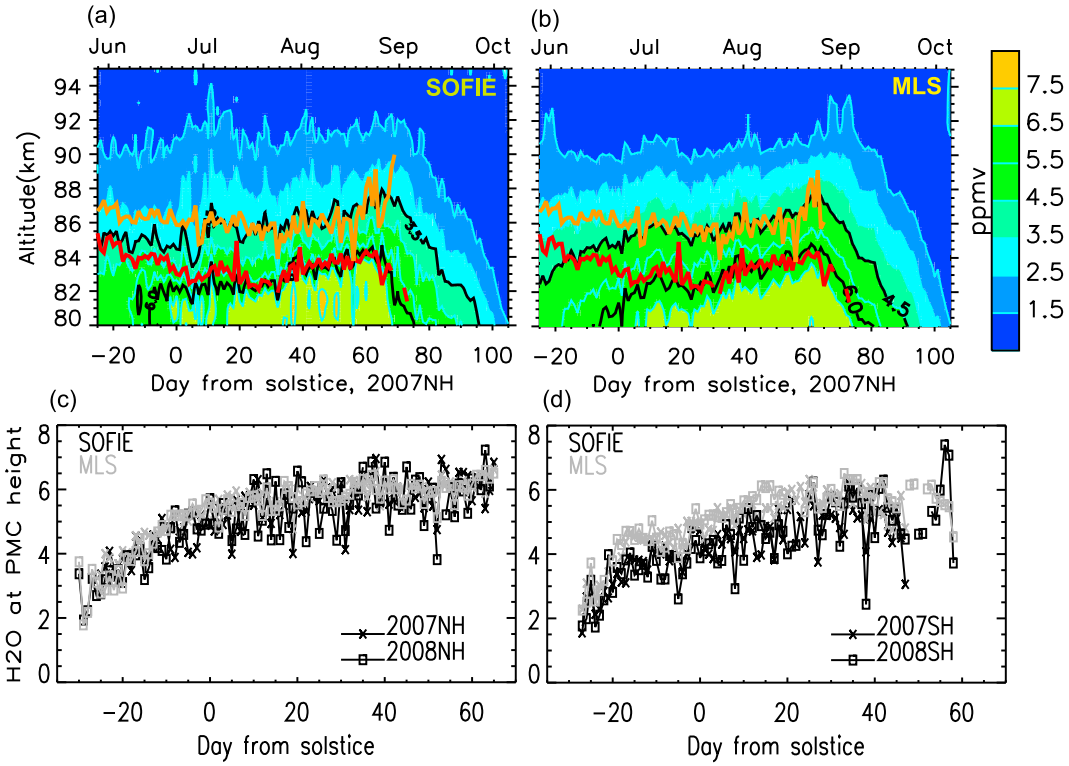

Figure 12. (a) Altitude versus time cross section of 2007 NH SOFIE H_2O focused on the upper mesosphere, with the SOFIE mesopause height (thick orange) and PMC height (thick red) superimposed. The thick black contours are for 3.5 and 6.0 ppmv, respectively. (b) Same as Figure 12a, except for MLS H_2O. The black contours are for 4.5 and 6.0 ppmv, respectively. MLS H_2O is averaged over SOFIE latitudes ±2.5° daily. (c) Time series of the daily zonal mean H_2O at SOFIE PMC heights in the NH. (d) Same as in Figure 12c, except for the SH.

and ~3.5 ppmv for PMC height; as the season progresses each height gradually merges with an isopleth of higher vmr value, i.e., ~3.5 ppmv for mesopause and ~6.0 ppmv for PMC height and remains so until the end of the PMC season. This two-stage evolution is not surprising since during mid-May to mid-June, relatively strong upward transport of H_2O persists over a broader vertical range of the mesosphere (as shown in Figure 11), which is responsible for the rapid buildup of H_2O at the PMC levels. After mid-June a high-gradient region is formed and remains in a quasi-steady state due to the approximate balance between the chemical dissociation and the advective and diffusive parts of the eddy effects. The intraseasonal variation of the gravity wave drag frequently disturbs the balanced state and results in the adjustment of the centroid height of the high gradient region. Figures 12a and 12b together indicate that the MLS and SOFIE H_2O show highly consistent features except for one discrepancy, i.e., at the mesopause height MLS H_2O is higher than SOFIE by ~1.0 ppmv throughout the season. This difference is due to a more rapid decrease of SOFIE H_2O right above the enhancement layer. It is likely associated with the ice particle production and corresponding H_2O reduction that is probably better observed in SOFIE owing to its higher vertical resolution (~2 km). A similar difference also exists between SOFIE and ACE-FTS (see Figure 3a).

[39] To further verify the findings shown in Figures 12a and 12b, the time series of H_2O at PMC heights for 2007 and 2008, and for SOFIE and MLS, are superimposed in Figures 12c–12d. In the NH the data show basically the same levels of H_2O regardless of year or data sets. Similar to what Figures 12a and 12b show, H_2O at the PMC heights increases toward ~6.0–6.5 ppmv, with the change prior to the solstice much more rapid than after, and it somewhat remains steady toward the end of the season. In the SH the data show very similar behavior except that MLS H_2O is higher than SOFIE by ~1.0 ppmv. This is expected since the low bias of SOFIE with respect to MLS in the SH has been discussed more than once above this point.

6. Summary and Conclusions

[40] SOFIE H_2O precision is the highest among the data sets used in this validation study. In the vertical range 45–80 km SOFIE H_2O precision estimates are approximately 0.2%–2.5%, as compared to ~2%–4% for ACE-FTS H_2O, and ~4–34% for MLS H_2O. In the upper mesosphere at ~90 km the SOFIE estimated precisions degrade to ~20%.

[41] Comparisons of SOFIE H_2O with ACE-FTS and MLS in the NH mesosphere indicate overall very good agreement in all seasons. However, a significant bias exists between SOFIE and ACE-FTS in the NH summer at ~80 km where a layer of enhanced H_2O is observed by SOFIE. Although some of the ACE-FTS profiles do also have this layer, their mean effect indicates much weaker enhancement than in SOFIE H_2O. After applying the AK smoothing SOFIE and MLS show fairly good agreement around this

layer, which supports the argument that a broad enhancement layer of MLS H_2O in the altitude range ~65–80 km is very likely the reflection of such a layer. In the SH SOFIE H_2O vmr is systematically lower than both ACE-FTS and MLS H_2O vmr in all seasons, with a mean percentage difference of ~10%–20% below ~80 km.

[42] Altitude versus time cross sections of daily and zonal mean H_2O for SOFIE and MLS show overall excellent agreement in some key features of seasonal development and vertical distribution throughout the upper stratosphere and mesosphere. However, SOFIE shows a persistently drier SH (0.5–0.7 ppmv on average) after summer solstice while MLS shows a slightly wetter SH (0.2–0.5 ppmv on average) prior to 35 DFS and later shows comparable vmrs between the two hemispheres. The SOFIE observed CH_4 in the upper stratosphere to lower mesosphere (35–65 km) shows stronger depletion in SH in both 2007 and 2008, which supports a slightly wetter instead of a drier SH in this vertical range.

[43] The finer vertical resolution and year-round polar coverage of SOFIE H_2O provides a better opportunity to observe the upwelling in the polar summer mesosphere. The slopes of H_2O isopleths on an altitude versus time cross section are used to estimate the upwelling air motion. On the basis of a well-established theory and early model results [e.g., *Garcia and Solomon*, 1985; *Huang and Smith*, 1991], we find that, in a qualitative sense, these slopes correctly reflect the seasonal variation and the vertical distribution of the upwelling in the lower to middle mesosphere, and the magnitudes are also comparable. In the upper mesosphere, H_2O photodissociation becomes a dominant factor and the isopleth slope is no longer able to reflect the upwelling. The intraseasonal variation of the slopes suggests that from mid-May to mid-June in the NH the relatively strong upwelling persists in a broader vertical range of the mesosphere, while in July and August the upwelling weakens in the lower to middle mesosphere. The H_2O slopes in the SH summer are far from being similar to those in the NH summer. Instead, it suggests overall much weaker upwelling in the lower to middle mesosphere and meanwhile the maximal upwelling is reached in January rather than in December. Moreover, the SH case is less agreeable with the established theory in the regard that the slopes do not show a monotonic strengthening as altitude increases.

[44] For both SOFIE and MLS, the daily mean H_2O vmr at the polar mesospheric cloud (PMC) height or mesopause height increases rapidly prior to the solstice and then approaches a near-constant but slightly increasing level throughout the season. The similar intraseasonal variations after the solstice between the PMC height, mesopause height, and the height of the H_2O high-gradient region reflect the central role that gravity wave drag plays in determining the H_2O and temperature vertical distribution in polar summer.

[45] **Acknowledgments.** This work was accomplished at the Center for Atmospheric Sciences, Hampton University, Hampton, Virginia. Funding for the AIM mission was provided by NASA's Small Explorers Program under contract NAS5-03132. SOFIE was built by the Space Dynamics Laboratory (SDL) at Utah State University in Logan, Utah. We thank the AIM and SOFIE/AIM team members for their tireless support and advice. We are very grateful to the MLS/Aura data retrieval and science teams at JPL for making the MLS level 2 data available online for convenient download, and we especially thank Dr. Alyn Lambert for kindly providing MLS Averaging kernels (AKs). We thank the ACE-FTS retrieval team for providing the data in a timely manner. The Atmospheric Chemistry Experiment (ACE) on the SCISAT platform is a Canadian-led mission mainly supported by the Canadian Space Agency and the Natural Sciences and Engineering Research Council of Canada. Some support was also provided by the U.K. Natural Environment Research Council, NERC. We acknowledge the HALOE retrieval and science teams for making a special effort to develop the Vpmc algorithm and data set.

References

Andrews, D. G., J. R. Holton, and C. B. Leovy (1987), Middle atmosphere dynamics, in *International Geophysical Series*, vol. 40, p. 489, Academic, San Diego.

Bernath, P. F. (2006), Atmospheric Chemistry Experiment (ACE): Analytical chemistry from orbit, *Trend. Anal. Chem.*, *25*(7), 647–654.

Bernath, P. F., et al. (2005), Atmospheric chemistry experiment (ACE): Mission overview, *Geophys. Res. Lett.*, *32*, L15S01, doi:10.1029/2005GL022386.

Brasseur, G., and S. Solomon (2005), *Aeronomy of the Middle Atmosphere: Chemistry and Physics of the Stratosphere and Mesosphere*, 3rd ed., Springer, Dordrecht, Netherlands.

Carleer, M. R., et al. (2008), Validation of water vapour profiles from the Atmospheric Chemistry Experiment (ACE), *Atmos. Chem. Phys. Discuss.*, *8*, 4499–4559.

Garcia, R. R. (1989), Dynamics, radiation, and photochemistry in the mesosphere: Implications for the formation of noctilucent clouds, *J. Geophys. Res.*, *94*(D12), 14,605–14,615, doi:10.1029/JD094iD12p14605.

Garcia, R. R., and S. Solomon (1985), The effect of breaking gravity waves on the dynamics and chemical composition of the mesosphere and lower thermosphere, *J. Geophys. Res.*, *90*(D2), 3850–3868, doi:10.1029/JD090iD02p03850.

Garcia, R. R., D. R. Marsh, D. E. Kinnison, B. A. Boville, and F. Sassi (2007), Simulation of secular trends in the middle atmosphere, 1950–2003, *J. Geophys. Res.*, *112*, D09301, doi:10.1029/2006JD007485.

Gordley, L. L., B. T. Marshall, and D. A. Chu (1994), LINEPAK: Algorithms for modeling spectral transmittance and radiance, *J. Quant. Spectrosc. Radiat. Transfer*, *52*(5), 563–580, doi:10.1016/0022-4073(94)90025-6.

Gordley, L. L., et al. (2009), The solar occultation for ice experiment, *J. Atmos. Sol. Terr. Phys.*, *71*, 300–315, doi:10.1016/j.jastp.2008.07.012.

Froidevaux, L., et al. (2008), Validation of Aura Microwave Limb Sounder stratospheric ozone measurements, *J. Geophys. Res.*, *113*, D15S20, doi:10.1029/2007JD008771.

Harries, J. E., J. M. Russell III, A. F. Tuck, L. L. Gordley, P. Purcell, K. Stone, R. M. Bevilacqua, M. Gunson, G. Nedoluha, and W. A. Traub (1996), Validation of measurements of water vapor from the Halogen Occultation Experiment (HALOE), *J. Geophys. Res.*, *101*(D6), 10,205–10,216, doi:10.1029/95JD02933.

Hervig, M. E., L. L. Gordley, J. M. Russell III, S. Bailey, and G. Baumgarten (2009), Interpretation of SOFIE PMC measurements: Cloud identification and derivation of mass density, particle shape, and particle size, *J. Atmos. Sol. Terr. Phys.*, *71*(3–4), 316–330, doi:10.1016/j.jastp.2008.07.009.

Hoppel, K. W., N. L. Baker, L. Coy, S. D. Eckermann, J. P. McCormack, G. E. Nedoluha, and E. Siskind (2008), Assimilation of stratospheric and mesospheric temperatures from MLS and SABER into a global NWP model, *Atmos. Chem. Phys.*, *8*, 6103–6116.

Huang, T. Y. W., and A. K. Smith (1991), The mesospheric diabatic circulation and the parameterized thermal effect of gravity wave breaking on the circulation, *J. Atmos. Sci.*, *48*(8), 1093–1111.

Jensen, E., and G. E. Thomas (1988), A growth-sedimentation model of polar mesospheric clouds' comparison with SME measurements, *J. Geophys. Res.*, *93*(D3), 2461–2473, doi:10.1029/JD093iD03p02461.

Lambert, A., et al. (2007), Validation of the Aura Microwave Limb Sounder middleatmosphere water vapor and nitrous oxide measurements, *J. Geophys. Res.*, *112*, D24S36, doi:10.1029/2007JD008724.

Livesey, N. J., W. V. Snyder, W. G. Read, and P. A. Wagner (2006), Retrieval algorithms for the EOS Microwave Limb Sounder (MLS), *IEEE Trans. Geosci. Remote Sens.*, *44*, 1144–1155.

Livesey, N. J., et al. (2007), Version 2.2 level 2 data quality and description document, *Tech. Rep.*, Jet Propul. Lab., Pasadena, Calif.

Llewellyn, E. J., et al. (2004), The OSIRIS instrument on the Odin spacecraft, *Can. J. Phys.*, *82*, 411–422.

Marshall, B. T., L. L. Gordley, and D. A. Chu (1994), BANDPAK Algorithms for modeling broadband transmission and radiance, *J. Quant. Spectrosc. Radiat. Transfer*, *52*, 581–599.

McHugh, M., M. Hervig, B. Magill, R. E. Thompson, E. Remsberg, J. Wrotny, and J. M. Russell (2003), Improved mesospheric temperature, water vapor and polar mesospheric cloud extinctions from HALOE, *Geophys. Res. Lett.*, *30*(8), 1440, doi:10.1029/2002GL016859.

McIntyre, M. E. (1989), On dynamics and transport near the polar mesopause in summer, *J. Atmos. Sci.*, *94*, 14,617–14,628.

Murtagh, D., et al. (2002), An overview of the Odin atmospheric mission, *Can. J. Phys.*, *80*(4), 309–319.

Nassar, R., P. F. Bernath, C. D. Boone, G. L. Manney, S. D. McLeod, C. P. Rinsland, R. Skelton, and K. A. Walker (2005), Stratospheric abundances of water and methane based on ACE-FTS measurements, *Geophys. Res. Lett.*, *32*, L15S04, doi:10.1029/2005GL022383.

Rapp, M., F.-J. Lübken, and A. Müllemann (2002), Small-scale temperature variations in the vicinity of NLC: Experimental and model results, *J. Geophys. Res.*, *107*(D19), 4392, doi:10.1029/2001JD001241.

Remsberg, E. E., et al. (2008), Assessment of the quality of the Version 1.07 temperature versus pressure profiles of the middle atmosphere from TIMED/SABER, *J. Geophys. Res.*, *113*, D17101, doi:10.1029/2008JD010013.

Rodgers, C. D., and B. J. Connor (2003), Intercomparison of remote sounding instruments, *J. Geophys. Res.*, *108*(D3), 4116, doi:10.1029/2002JD002299.

Rosenfield, J. E., M. R. Schoeberl, and M. A. Geller (1987), A computation of the stratospheric diabatic circulation using an accurate radiative transfer model, *J. Atmos. Sci.*, *44*, 859–876.

Russell, J. M., III, L. L. Gordley, J. H. Park, S. R. Drayson, D. H. Hesketh, R. J. Cicerone, A. F. Tuck, J. E. Frederick, J. E. Harries, and P. Crutzen (1993), The halogen occultation experiment, *J. Geophys. Res.*, *98*(D6), 10,777–10,797, doi:10.1029/93JD00799.

Russell, J. M., III, M. G. Mlynczak, L. L. Gordley, J. J. Tansock, and R. W. Esplin (1999), Overview of the SABER experiment and preliminary calibration results, in *Optical Spectroscopic Techniques and Instrumentation for Atmospheric and Space Research III*, edited by A. M. Larar, *Proc. SPIE*, 3756, 277–288.

Russell, J. M., III, et al. (2009), The Aeronomy of Ice in the Mesosphere (AIM) mission: Overview and early science results, *J. Atmos. Sol. Terr. Phys.*, *71*(3–4), 289–299, doi:10.1016/j.jastp.2008.08.011.

Stevens, M. H., R. R. Conway, C. R. Englet, M. E. Summers, K. U. Grossmann, and O. A. Gusev (2001), PMCs and the water frost point in the Arctic summer mesosphere, *Geophys. Res. Lett.*, *28*(23), 4449–4452, doi:10.1029/2001GL013598.

Stevens, M. H., R. L. Gattinger, J. Gumbel, E. J. Llewellyn, D. A. Degenstein, M. Khaplanov, and G. Witt (2008), First UV satellite observations of mesospheric water vapor, *J. Geophys. Res.*, *113*, D12304, doi:10.1029/2007JD009513.

Summers, M. E., R. R. Conway, C. R. Englert, D. E. Siskind, M. J. McHugh, M. H. Stevens, J. M. Russell, L. L. Gordley, and M. J. McHugh (2001), Discovery of a water vapor layer in the arctic summer mesosphere: Implications for polar mesospheric clouds, *Geophys. Res. Lett.*, *28*(18), 3601–3604, doi:10.1029/2001GL013217.

Waters, J. W., et al. (2006), The Earth Observing System Microwave Limb Sounder (EOS MLS) on the Aura satellite, *IEEE Trans. Geosci. Remote Sens.*, *44*, 1075–1092.

Wrotny, J. E., and J. M. Russell III (2006), Interhemispheric differences in polar mesospheric clouds observed by the HALOE instrument, *J. Atmos. Sol. Terr. Phys.*, *68*(12), 1352–1369, doi:10.1016/j.jastp.2006.05.014.

von Zahn, U., and U. Berger (2003), Persistent ice cloud in the midsummer upper mesosphere at high latitudes: Three-dimensional modeling and cloud interactions with ambient water vapor, *J. Geophys. Res.*, *108*(D8), 8451, doi:10.1029/2002JD002409.

P. F. Bernath, Department of Chemistry, University of York, Heslington, York YO10 5DD, UK.

L. Deaver and L. L. Gordley, GATS, Inc., 11864 Canon Blvd., Ste. 101, Newport News, VA 23606, USA.

M. E. Hervig, GATS, Inc., 65 South Main St., Driggs, ID 83422, USA.

P. P. Rong and J. M. Russell III, Center for Atmospheric Sciences, Hampton University, Hampton, VA 23668, USA. (ping-ping.rong@hamptonu.edu)

K. A. Walker, Department of Physics, University of Toronto, 60 St. George St., Toronto, ON M5S 1A7, Canada.